From these observations we conclude the following. First, unmyelinated afferent fibers of the somatic nerves follow general rules for central termination that also apply to myelinated fibers. (i) The termination of the functionally defined kinds of sensory unit appears in a specific region of the spinal gray matter; (ii) the termination pattern of each functionally defined kind of C-fiber sensory unit appears to be characteristic, although regional differences in spinal cord organization, such as those distinguishing cervical from lumbar levels, can influence the pattern. Second, the superficial layers of the spinal dorsal horn—particularly lamina II, the substantia gelatinosa—appear to be the main projection zone for unmyelinated primary afferent fibers from the skin. (Whether this area is also a termination zone for C-afferent units from visceral and other subcutaneous tissues is unknown.) This result is consistent with deductions based on indirect evidence from classical morphological analyses and correlations between functional properties and dendritic arborization of spinal neurons (*8, 11*). Third, a given unmyelinated primary afferent fiber in a central termination zone can have significantly different size enlargements appearing along its course. The size variation may be in the en passant enlargements themselves or between the terminal bouton and the en passant varicosities, a point noted in the past for one type of myelinated sensory axon (*9*). Some en passant enlargements along a collateral were noted to be 0.5 μm in diameter while others were over 2 μm in diameter. Not all branches of an arborization showed such variation in enlargement size. The latter observation suggests that different kinds of synaptic contacts may be made by a given fiber.

REFERENCES AND NOTES

1. A. G. Brown, P. K. Rose, P. J. Snow, *J. Physiol. (London)* **277**, 15 (1978); A. R. Light and E. R. Perl, *J. Comp. Neurol.* **186**, 133 (1979).
2. E. R. Perl, in *Neural Mechanisms of Pain*, L. Kruger and J. C. Liebeskind, Eds., vol. 6 in *Advances in Pain Research and Therapy* (Raven Press, New York, 1984), pp. 23–51; Y. Sugiura, E. Schrank, E. R. Perl, *Soc. Neurosci. Abstr.* **11**, 118 (1985).
3. C. R. Gerfen and P. E. Sawchenko, *Brain Res.* **290**, 219 (1984); G. J. Ter Horst, H. J. Groenewegen, H. Karst, P. G. M. Luiten, *ibid.* **307**, 379 (1984).
4. P. R. Burgess and E. R. Perl, in *Handbook of Sensory Physiology: Somatosensory System*, A. Iggo, Ed. (Springer-Verlag, Berlin, 1973), vol. 2, pp. 29–78; P. Bessou and E. R. Perl, *J. Physiol. (Paris) Suppl. 1* **60**, 218 (1968); M. Réthelyi and J. Szentagothai, *Exp. Brain Res.* 7, 258 (1969).
5. V. Shea and E. R. Perl, *J. Neurophysiol.* **54**, 491 (1985).
6. S. M. Hsu, L. Raine, H. Fanger, *Am. J. Clin. Pathol.* **75**, 734 (1981); *J. Histochem. Cytochem.* **29**, 577 (1981).
7. J. J. Capowski and M. Réthelyi, *Brain Theory Newsl.* **3**, 179 (1978).
8. M. Réthelyi, *J. Comp. Neurol.* **172**, 511 (1977); ______ and J. Szentagothai, *Exp. Brain Res.* 7, 258 (1969).
9. M. Réthelyi, A. R. Light, E. R. Perl, *J. Comp. Neurol.* **207**, 381 (1982).
10. M. E. Scheibel and A. B. Scheibel, *Brain Res.* **13**, 417 (1969).
11. S. W. Ranson, *Am. J. Anat.* **16**, 97 (1914); *Brain* **38**, 381 (1915); K. M. Earle, *J. Comp. Neurol.* **96**, 93 (1952); S. Gobel and J. M. Binck, *Brain Res.* **132**, 347 (1977); A. R. Light, D. L. Trevino, E. R. Perl, *J. Comp. Neurol.* **186**, 151 (1979); For review, see E. R. Perl, in (*2*).
12. B. Rexed, *J. Comp. Neurol.* **96**, 415 (1952).

13. Supported by a grant from the National Institute of Neurological and Communicative Disorders and Stroke (NS 10321). Computer facilities provided by grant NS 14899 from NINCDS. J. Azerad and E. Schrank helped to develop the recording techniques and participated in the preliminary experiments in which attempts were made to use HRP as a marker. We thank D. Maloof for his aid in preparing and editing the manuscript.

14 May 1986; accepted 12 August 1986

The Little Ice Age as Recorded in the Stratigraphy of the Tropical Quelccaya Ice Cap

L. G. THOMPSON, E. MOSLEY-THOMPSON, W. DANSGAARD, P. M. GROOTES

The analyses of two ice cores from a southern tropical ice cap provide a record of climatic conditions over 1000 years for a region where other proxy records are nearly absent. Annual variations in visible dust layers, oxygen isotopes, microparticle concentrations, conductivity, and identification of the historical (A.D. 1600) Huaynaputina ash permit accurate dating and time-scale verification. The fact that the Little Ice Age (about A.D. 1500 to 1900) stands out as a significant climatic event in the oxygen isotope and electrical conductivity records confirms the worldwide character of this event.

IN 1983 TWO ICE CORES, ONE 154.8-M summit core containing a record of 1350 years and another 163.6-m core (core 1) containing a record of 1500 years, were recovered from the Quelccaya ice cap (13°56′S, 70°50′W) with a solar-powered drilling system. About 6000 samples, cut from pits, shallow cores, and the two deep cores were melted in closed containers by passive solar heating in a laboratory tent, placed in polyethylene bottles, sealed with wax, and shipped to Ohio State University. Samples were divided so that microparticle concentrations, size distributions, conductivity, and oxygen isotope ($\delta^{18}O$) measurements could be made on identical samples. Total β radioactivity and pollen and chemical analyses were conducted for 1500 samples. The microparticle and conductivity measurements were made under class 100 clean-room conditions at the Ohio State University, and $\delta^{18}O$ analyses on the summit core were conducted at the University of Copenhagen and on core 1 at the University of Washington. We discuss the 1000-year record, since A.D. 1000, of microparticle concentrations, conductivities, and oxygen isotopes (*1–3*).

Dating of the ice cap cores was accomplished by using several stratigraphic features that exhibit seasonal variability. The initial age for the bottom of the ice cap was estimated from flow-model calculations (*4*) that depend heavily on initial assumptions and boundary conditions. Alternative stratigraphic dating of the core was made possible in the field by examination of visible annual dust layers (Fig. 1) (*1*). The thickness of the annual layers ranged from 1.24 m (ice equivalent) at the surface to 0.01 m at the base. In both cores, the visible stratigraphy was complemented by the preservation of annual variations in microparticle concentrations, conductivity, and oxygen isotope ratios (Fig. 1). The combination of ice core parameters exhibiting seasonal cycles allows clarification of ambiguous features and results in the most reliable time scale. Further time scale refinement results when the two core records are compared.

In general, visible dust layers, characteristic of the dry season (*3*), are associated with high microparticle concentrations, less negative $\delta^{18}O$ ratios, and high conductivities. Increased dry-season particle concentrations are attributed to (i) receipt of intense radiation accompanied by little accumulation (minor sublimation, which leaves the insoluble particles concentrated at the surface); (ii) dominant wind direction from the west and northwest, which transports material from the high, dry altiplano; and (iii) higher dry-season wind speeds, which facilitate entrainment and transportation.

L. G. Thompson and E. Mosley-Thompson, Institute of Polar Studies, Ohio State University, Columbus, OH 43210.
W. Dansgaard, Geophysical Institute, Department of Glaciology, University of Copenhagen, Haraldsgade 6, Copenhagen 2200, Denmark.
P. M. Grootes, Quaternary Isotope Laboratory, University of Washington, Seattle, WA 98195.

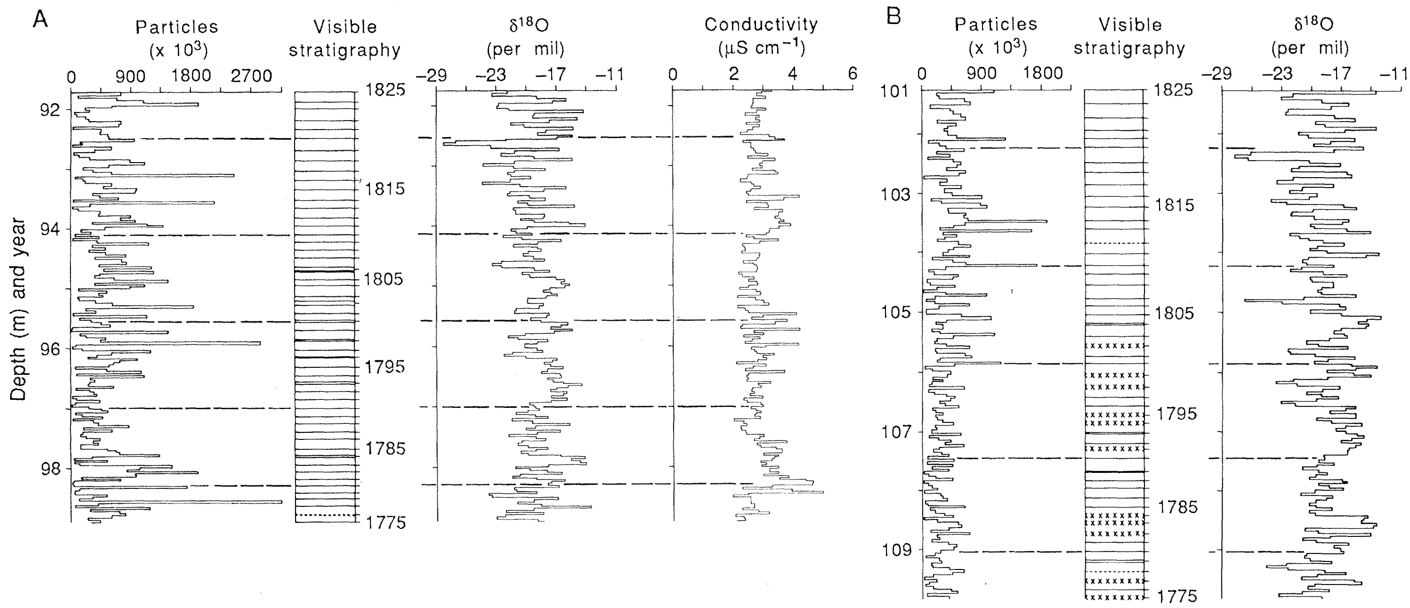

Fig. 1. The stratigraphic parameters used to date the summit core (A) and core 1 (B), 1775–1825. Annual signals are recorded in microparticle concentrations (particles from 0.63 to 16.0 μm in diameter per milliliter of sample), oxygen isotopes, conductivity (summit core only), and visible stratigraphy. For stratigraphy, a single solid line represents a normal dry-season dust layer; a single dashed line and a double dashed line represent very light and light dust layers, respectively. Series of x's symbolize diffuse dry-season layers. The most negative $\delta^{18}O$ values measured in both cores occurred between July 1819 and July 1820 after a series of years when the wet-season $\delta^{18}O$ values were unusually negative, possibly reflecting a global perturbation caused by the 1815 eruption of Tambora (*17*).

The oxygen isotopic composition exhibits an annual cycle with least negative values associated with winter snowfall (*5*). Summer snow is isotopically light, although occasional significant short-term $\delta^{18}O$ variations within a single year make it difficult to identify annual cycles in the oxygen isotope stratigraphy alone (*3*). This is also true for the annual variations in microparticle concentrations and conductivity. Ambiguities in identifying the annual signal from a single parameter are resolved by integrating the records.

The time scale has been verified by the identification (in both cores) of an ash attributed to Huaynaputina (16°35′S, 70°52′W), the largest historically recorded volcanic eruption in southern Peru. During the eruptive phase, 19 February to 6 March 1600 (*6*), there was total darkness for 7 days in Arequipa (16°25′S, 71°32′W), 80 km to the northwest, and houses collapsed under the weight of ash accumulating on the roofs (*7*). The ash was widely distributed (*8*) and may have reached northward 3000 km to Nicaragua. In the past 1000 years the Quelccaya cores record one prominent dust event (Fig. 2), which is best shown by the major increase in large (diameter ≥1.59 μm) insoluble particles.

An ash sample collected from an archeological site, Cerro Trapiche (17°11′S, 70°58′W), near Moquegua is thought to be from the Huaynaputina eruption. The x-ray energy-dispersive spectra (Trachor Northern) (Fig. 3, A–C) and scanning electron microscope (Cambridge S4–10) micrographs (Fig. 3, D–G) show the similarities between the volcanic ash from the archeological site (Fig. 3D) and that from both ice cores (Fig. 3, F and G). Similarly, the natural background material (Fig. 3E) found throughout most of the Quelccaya cores consists of rounded windblown clay particles derived from the surrounding altiplano. In the energy-dispersive spectra (Fig. 3, A–C), the step graphs and dots represent the archeological ash and ice core particulates, respectively. For both cores, the composition of the volcanic material (Fig. 3, B and C), consisting principally of glassy shards (Fig. 3, F and G), is similar to the ash collected at Cerro Trapiche (Fig. 3D), whereas the spectrum for the background material (Fig. 3A) is different. Initially from visual stratigraphy, we dated this peak at 1597, but the final chronology from visible stratigraphy, $\delta^{18}O$ values, and microparticle concentrations places the event at 1600. The

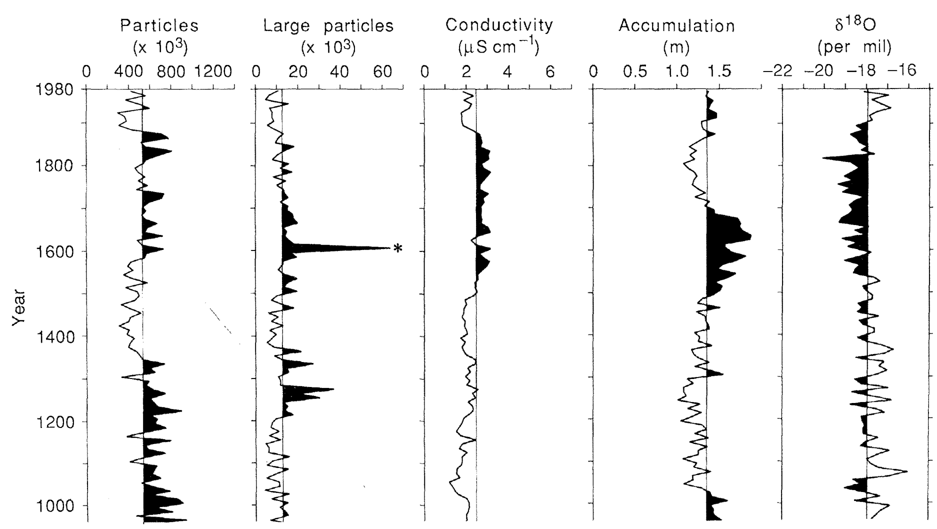

Fig. 2. Decadal variations in microparticle concentrations (total particles ≥0.63 to 16.0 μm and large particles >1.59 μm in diameter, per milliliter of sample), conductivity, oxygen isotopic ratios, and net accumulation for the past 1000 years. The accumulation record is taken from core 1 (*1*). The solid line represents the 1000-year average. The "Little Ice Age" (1500–1900) stands out clearly in the $\delta^{18}O$ and conductivity records as a major climatic event in tropical South America.

similarity in morphology and elemental compositions, in conjunction with the date of the ice layer containing the ash, leads us to conclude that Huaynaputina is the source of the volcanic particles preserved in the 1600 horizon of both ice cores.

Thus, annual variation in microparticles and oxygen isotopes, along with the known 1600 Huaynaputina eruption, have been used to refine the visual stratigraphic time scale. The Quelccaya cores have been dated back to 1500 with an estimated uncertainty of ±2 years and an absolute date at 1600. The dating of the lower sections of both cores is based solely on the visible dust layers recorded in the field; it has an estimated uncertainty of ±20 years.

The Little Ice Age recorded in the Northern Hemisphere earlier in this millennium was characterized by colder temperatures and expanded glaciers. Its dates determined from historical and proxy climate records vary depending on location and observed parameter. For example, the following Little Ice Age intervals have been quoted (*9–11*): 1430–1850, 1550–1800, 1550–1850, 1550–1700, and 1500–1800.

An obvious question is how well the larger-scale events are recorded in these tropical ice cores. Figure 4A illustrates the Northern Hemisphere decadal temperature departures from the 1881–1975 mean (*12*), compiled by Groveman and Landsberg (*13*), from long temperature series including Manley's central England temperature record back to 1658 and from proxy data including freeze records and tree rings before 1658. Therefore, uncertainties in this record are larger in the earlier years (*14*). The $\delta^{18}O$ decadal averages for summit core and core 1 are shown in Fig. 4, B and C, as departures from their respective 1880–1980 means. The excellent agreement (slope = 0.89 ± 0.04, n = 40) between the two $\delta^{18}O$ records for 40 decades suggests a lack of glaciological noise, which implies that much of the variability represents an atmospheric input signal. In addition, the similarity of the $\delta^{18}O$ records confirms field observations of uniform accumulation at these two sites.

Although inferences about temperature from $\delta^{18}O$ records must be made cautiously (as $\delta^{18}O$ also reflects changes in both water-vapor history and snow surface processes), and, although the average decadal $\delta^{18}O$

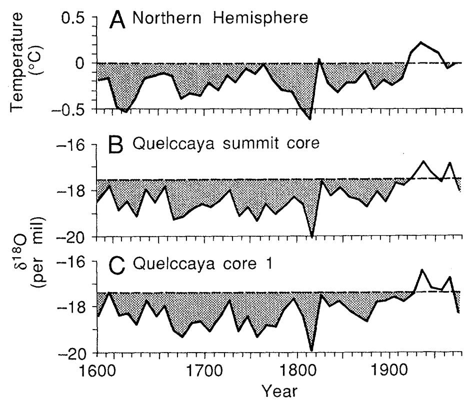

Fig. 4. Decadal temperature departures (from the 1881–1975 mean) in the Northern Hemisphere (*13*) from 1580 to 1975 compared with decadal average $\delta^{18}O$ values for both Quelccaya ice cores. The dashed line is the 1880–1980 mean.

values reflect mainly summer atmospheric conditions [as more than 80% of the annual precipitation falls in the wet season (*15*)], the Northern Hemisphere mean temperature departures and the Quelccaya summit core $\delta^{18}O$ record are well linearly related (*16*). This linear relation is best, as would be expected, for the latter part of the temperature record (1770–1980), which is based on more stations and better-documented observations (*16*). This relation is the more remarkable as the Quelccaya records represent a single Southern Hemisphere site, whereas the temperature record is based on a maximum of nine primarily high latitude Northern Hemisphere sites.

Particularly striking (Fig. 4) is the association of the very cold period (1800–1820) in the Northern Hemisphere temperature record with the decades of most negative $\delta^{18}O$ values in the Quelccaya cores, which suggests that this cold period was part of a global climate anomaly. Similarly, the warm period between 1920 and 1940 (Fig. 4A) is accompanied by less negative $\delta^{18}O$ values (Fig. 4, B and C).

Figure 2 illustrates the decadal averages of microparticle concentrations, conductivity, oxygen isotopic ratio, and ash accumulation for the past 1000 years from the summit core. As the $\delta^{18}O$ profile is significantly correlated with Northern Hemisphere temperature, as long ago as the data reach (Fig. 4), it is reasonable to associate the period of generally low $\delta^{18}O$ values between 1530 and 1900 with the Little Ice Age (Fig. 2). During most of the Little Ice Age in southern Peru, microparticle concentrations and conductivity were 20 to 30% above their respective averages during the 14th, 15th, and 20th centuries, whereas around 1700 the accumulation changed from above average to below average (Fig. 2). The initial increases in the decadal averages for conduc-

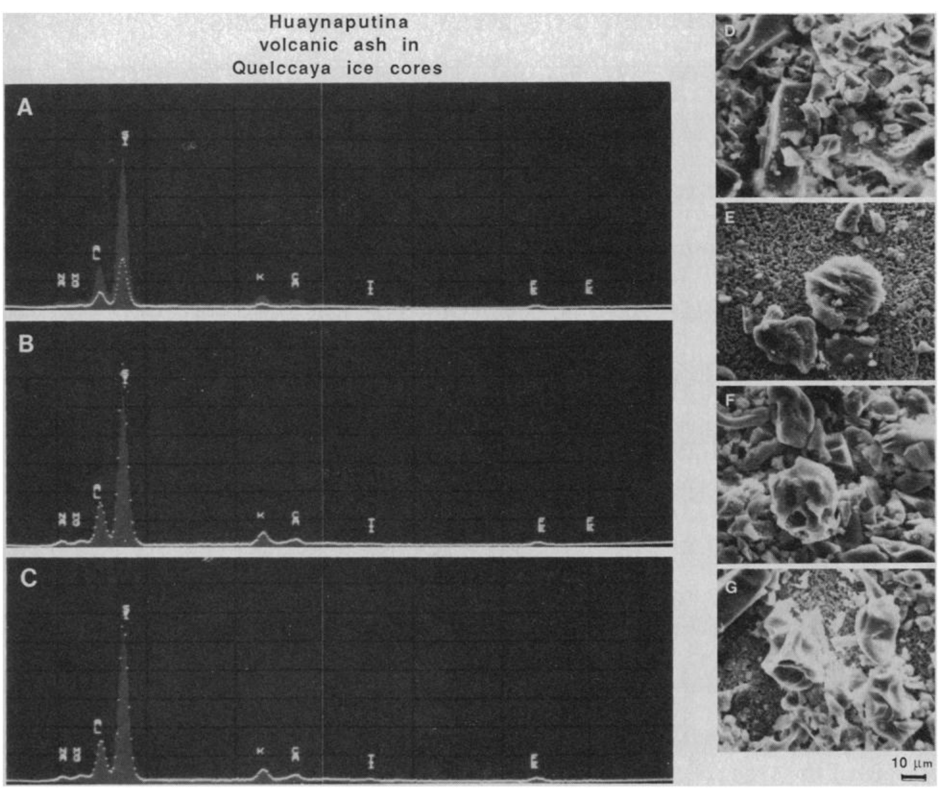

Fig. 3. (A–C) X-ray energy-dispersive spectra. (D–G) Scanning electron microscope micrographs. (D) Huaynaputina ash from an archeological site. (E) Particulates from 1592, representing a pre-Huaynaputina horizon in summit core. (F) The 1600 ash layer from the summit core. (G) The 1600 ash layer from core 1. In all elemental comparisons (A–C) (*18*), the archeological Huaynaputina ash is illustrated by the step graph and the material from the ice cores by the dots. These data show (i) the marked difference in structure and elemental composition between the Huaynaputina ash and the natural background particulates derived from the surrounding altiplano and (ii) the identical characteristics of the material collected at the archeological site and that recovered from the 1600 horizon in both Quelccaya cores.

tivity and accumulation began 30 years before the decrease in the $\delta^{18}O$ record.

Increases in particulates may have resulted from increased atmospheric impurities, decreased accumulation, or both. The accumulation history from Quelccaya (*1*) suggests that the increase in particulates at the onset of the Little Ice Age must be due to increased atmospheric loading, not decreased accumulation. The 1500–1720 interval was the wettest in the 1000-year record, whereas the 1720–1860 interval was very dry; nonetheless, the dry-period microparticle concentration and conductivity values are similar to those from the preceding wet period. Preliminary scanning electron and light-microscopic analyses show no significant changes in the types of particles deposited during the Little Ice Age. Therefore, the observed increase in particulate deposition is attributed to increased wind velocities across the high altiplano of southern Peru.

Ice core data provide a record of several facets of past variations in the earth's atmosphere, although that record, like all proxy climate records, represents a complex integration of both local and large-scale processes. The Quelccaya ice core records provide a well-dated climatic record of the Little Ice Age in the tropics of South America and support the growing body of evidence that the Little Ice Age was a global event.

REFERENCES AND NOTES

1. L. G. Thompson, E. Mosley-Thompson, J. F. Bolzan, B. R. Koci, *Science* **229**, 971 (1985).
2. L. G. Thompson, S. Hastenrath, B. Morales Arnao, *ibid.* **203**, 1240 (1979); L. G. Thompson, *J. Glaciol.* **25**, 69 (1980).
3. L. G. Thompson, E. Mosley-Thompson, P. M. Grootes, M. Pourchet, S. Hastenrath, *J. Geophys. Res.* **89**, 4638 (1984).
4. L. G. Thompson *et al.*, *J. Glaciol.* **28**, 57 (1982).
5. L. G. Thompson and W. Dansgaard, *Antarct. J. U.S.* **10**, 24 (1975).
6. T. Simkin *et al.*, *Volcanoes of the World* (Hutchinson Ross, Stroudsburg, PA, 1981).
7. Anonymous, *Moquegua, Informe del Peru* (Promotora Editorial Latinoamericana, Newton-Cortazar, Lima, 1976), vol. 7, part 8; F. M. Bullard, *Bull. Volcanol.* **24**, 443 (1962); P. Francis, *Volcano News* 7, 4 (1981).
8. A. Vazquez de Espinosa, *Smithson. Misc. Collect.* (C. U. Clark, transl.) **102**, 497 (1942).
9. J. R. Bray, *Science* **171**, 1242 (1971); A. Robock, *ibid.* **206**, 1402 (1979); V. Cermak, *Palaeogeogr. Palaeoclimatol. Palaeoecol.* **10**, 1 (1971); H. Flohn and R. Fantechi, *The Climate of Europe: Past, Present and Future* (Reidel, Dordrecht, 1984); H. H. Lamb, *Climate: Present, Past and Future*, vol. 2, *Climatic History and the Future* (Methuen, London, 1977); C. J. E. Schuurmans, in *Climatic Variations and Variability: Facts and Theories*, A. Berger, Ed. (Reidel, Dordrecht, 1981), pp. 245–258; R. G. Barry, in *Climatic Change and Variability: A Southern Perspective*, A. B. Pittock, L. A. Frakes, D. Jenssen, S. A. Peterson, J. W. Zillman, Eds. (Cambridge Univ. Press, Cambridge, England, 1978), pp. 150–166; C. D. Schonwiese, *Klimaschwankungen* (Springer-Verlag, Berlin, 1978).
10. J. Gribben and H. H. Lamb, in *Climatic Change*, J. Gribben, Ed. (Cambridge University Press, Cambridge, England, 1978), pp. 68–82.
11. H. H. Lamb, in *Climatic Changes on a Yearly to Millennial Basis*, N. A. Mörner and W. Karlén, Eds. (Reidel, Dordrecht, 1984), pp. 225–240; H. H. Lamb, *ibid.*, pp. 309–329.
12. I. Borzenkova, K. Ya. Vinnikov, L. P. Spirina, P. I. Stechnowskii, *Meteorol. Gidrologiva* 7, 27 (1976).
13. B. S. Groveman and H. E. Landsberg, *Geophys. Res. Lett.* **6**, 767 (1979).
14. H. E. Landsberg, in *Paleoclimate Analysis and Modeling*, A. D. Hecht, Ed. (Wiley, New York, 1985), pp. 27–70.
15. A. M. Johnson, *World Survey of Climatology, Climates of Central and South America*, W. Schwerdtfeger, Ed. (Elsevier, Amsterdam, 1976), vol. 12, p. 147.
16. As a measure of the linear relation between the $\delta^{18}O$ records in summit core and core 1, the slope and the SE of the slope were calculated (slope = 0.89 ± 0.04, *n* = 40). A perfectly linear relation would have a slope of unity and SE of zero. For the past 21 decades (1770–1980), the better-documented part of the temperature record, the slope is 0.95 ± 0.06 (*n* = 21), and the elimination of the decade with a prominent departure (1810–1820) makes little difference (slope = 0.94 ± 0.08, *n* = 20). The linear relation between each of the two ice-core $\delta^{18}O$ records and temperatures in the Northern Hemisphere has been characterized by the slope; however, the difference in the units of measure and the lack of an empirical relation between $\delta^{18}O$ and temperature makes the slope more difficult to interpret. Nevertheless, the nonzero slope and the low SE attest to the similarity between the ice core $\delta^{18}O$ records and the Northern Hemisphere temperature history (summit core: slope = 0.17 ± 0.03, *n* = 40; core 1: slope = 0.14 ± 0.03, *n* = 40). For the better-documented part of the temperature record (1770–1820), the linear relations are (i) summit core (slope = 0.22 ± 0.04, *n* = 21) and (ii) core 1 (slope = 0.20 ± 0.04, *n* = 21).
17. R. B. Stothers, *Science* **224**, 1191 (1984).
18. All x-ray energy-dispersive spectra were obtained under identical instrumental conditions. Accelerating potential was 20 kV, count rates were 2000 counts/sec, and the spectra were accumulated for 100 seconds.

19. Supported by NSF grants ATM75-15513A02, ATM78-1609A01, ATM81-05079A02, and ATM82-13601A02. The NSF Division of Polar Programs (NSF-DPP) supported 1974 field investigations (GV41411) and development of the solar-powered drill. The Quaternary Isotope Laboratory (University of Washington) oxygen isotope study was supported by NSF grants DPP-8019756 and DPP-8400574, and that of the Geophysical Institute (University of Copenhagen) by the Danish Natural Science Research Council. We thank the Polar Ice Coring Office, Electroperu, and the Inter-American Geodetic Survey for their support. We thank the many people who have participated in the field programs; M. E. Moseley and R. A. Feldman for the Huaynaputina ash sample from Cerro Trapiche and for many valuable discussions, M. Davis for assistance in the laboratory and energy-dispersive analysis, J. Bolzan for comments on the manuscript, A. Leonardi for energy-dispersive analysis, J. Paskievitch for assistance in data analysis, K. Doddroe for typing, and R. Tope for the illustrations. Contribution 548 of the Institute of Polar Studies, Ohio State University.

23 January 1986; accepted 27 June 1986

Amino Acid Sequences Common to Rapidly Degraded Proteins: The PEST Hypothesis

SCOTT ROGERS, RODNEY WELLS, MARTIN RECHSTEINER

The amino acid sequences of ten proteins with intracellular half-lives less than 2 hours contain one or more regions rich in proline (P), glutamic acid (E), serine (S), and threonine (T). These PEST regions are generally, but not always, flanked by clusters containing several positively charged amino acids. Similar inspection of 35 proteins with intracellular half-lives between 20 and 220 hours revealed that only three contain a PEST region. On the basis of this information, it was anticipated that caseins, which contain several PEST sequences, would be rapidly degraded within eukaryotic cells. This expectation was confirmed by red blood cell–mediated microinjection of ^{125}I-labeled caseins into HeLa cells where they exhibited half-lives of less than 2 hours. The rapid degradation of injected α- and β-casein as well as the inverse correlation of PEST regions with intracellular stability indicate that the presence of these regions can result in the rapid intracellular degradation of the proteins containing them.

One of the generalizations to emerge from studies on protein secretion and organelle biogenesis is that portions of the amino acid sequence comprising a protein can specify its ultimate location within the cell (*1–3*). Selective degradation of intracellular proteins—the sorting of a protein out of existence—might be considered the ultimate in targeting. Here we report an observation that emerged from a survey of the literature: proteins that are rapidly degraded within eukaryotic cells contain regions rich in proline (P), glutamic acid (E), serine (S), and threonine (T).

Table 1 contains a list of the most rapidly degraded eukaryotic proteins of known sequence, their half-lives, and the amino acid regions (PEST) whose features are shared among the members of the set. Common to all PEST regions are high local concentrations of P, E, S, or T and to a lesser extent aspartic acid. To identify PEST regions by computer, we combined specific enrichment for these amino acids with several other features in an algorithm, PEST-SCORE, for ranking stretches of protein sequence (*4*). Scores for each PEST region in rapidly degraded proteins are listed in Table 1.

PEST regions begin and end with positively charged residues (Fig. 1), but internal lysine, arginine, and histidine residues are

Departments of Biology and Biochemistry, University of Utah, Salt Lake City, UT 84112.